ELECTRONIC SUPPLEMENTARY INFORMATION

Exchange Interactions in Photoinduced Magnetostructural States of Copper(II)-Nitroxide Spin Dyads

Sergey V. Tumanov,[a,b] Sergey L. Veber,[a,b] Svyatoslav E. Tolstikov,[a] Natalia A. Artiukhova,[a] Victor I. Ovcharenko[a] and Matvey V. Fedin*[a,b]

[a]International Tomography Center SB RAS, Institutskaya Str. 3a, 630090 Novosibirsk, Russia

[b]Novosibirsk State University, Pirogova Str. 2, 630090 Novosibirsk, Russia

E-mail: mfedin@tomo.nsc.ru

Table of Contents

1. Mid-IR spectrum of II measured in dark and after irradiation. Temperature dependence of the integrals of characteristic absorption lines displaying SS→WS conversion

The IR spectra of polycrystalline powders of the studied compounds placed on KBr pellet were recorded in the range of 4000–700 cm^{-1} (mid-IR) at T = 5–30 K using an FTIR spectrometer Bruker Vertex 80v (Bruker Optics, Germany) equipped with a continuous flow liquid He cryostat Oxford OptistatCF and with a liquid N_2 cooled MCT detector. The spectral resolution was 0.5 cm^{-1}. The sample was thermally equilibrated for 3 min for each temperature dependent measurement. The irradiation was achieved by using 730 nm LED placed in front of the cryostat window.

There are several characteristic vibrational lines reflecting SS→WS magnetostructural transitions (Fig. S1. FTIR spectra of **II** (1250 – 1700 cm-1 region) before and after irradiation with 730 nm LED. Highlighted areas show the integrals of characteristic lines which were used to trace the WS→SS conversion.1). Fig. S shows temperature-induced changes of the highlighted characteristic lines. If an integration region is chosen so that it does not include interference of several vibrational bands, it can be used to estimate the dynamics of WS→SS conversion. All of the highlighted lines clearly indicate that there are no WS→SS conversion under 10-5-10 K temperature loop.

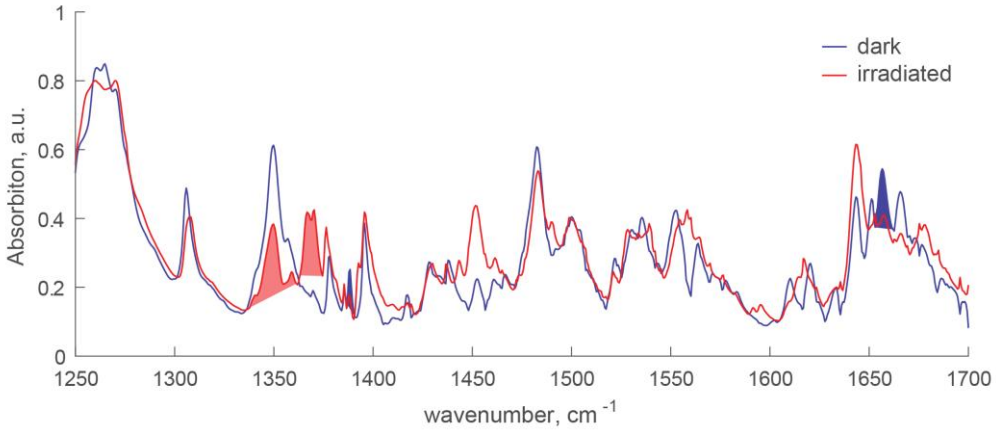

Fig. S1. FTIR spectra of **II** (1250 – 1700 cm^{-1} region) before and after irradiation with 730 nm LED. Highlighted areas show the integrals of characteristic lines which were used to trace the WS→SS conversion.

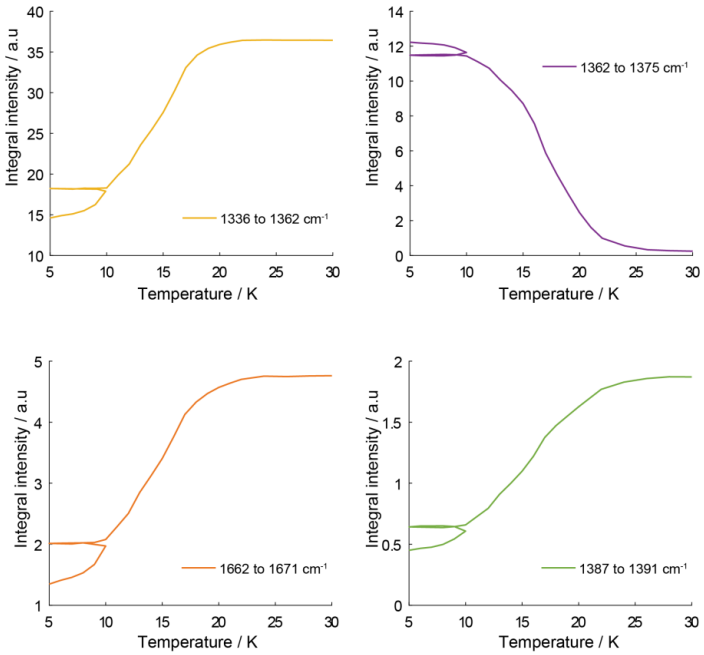

Fig. S2. Integral intensity of characteristic lines corresponding to WS↔SS transition of **II** in FTIR experiments.

2. EPR spectra of I and II measured at 5 K in dark, under irradiation of light and with subsequent temperature changes. Comparison of EPR spectra of I measured at 250 K and 5 K

Continuous wave (CW) EPR measurements were carried out at the X-band (≈9.7 GHz) using a commercial EPR spectrometer Bruker Elexsys E580 equipped with an Oxford Instruments temperature control system (T = 4–300 K). The temperature resolution was 1 K and thermal equilibrium was achieved by staying at every thermal point for 3-5 minutes. Other technical details are given in the main text.

Figure S3 shows EPR spectra of **I** in thermal SS and WS states. WS state corresponds to a single line. Due to the intercluster exchange interaction between the copper-nitroxide clusters in triplet state there is no half-field line at high temperatures.

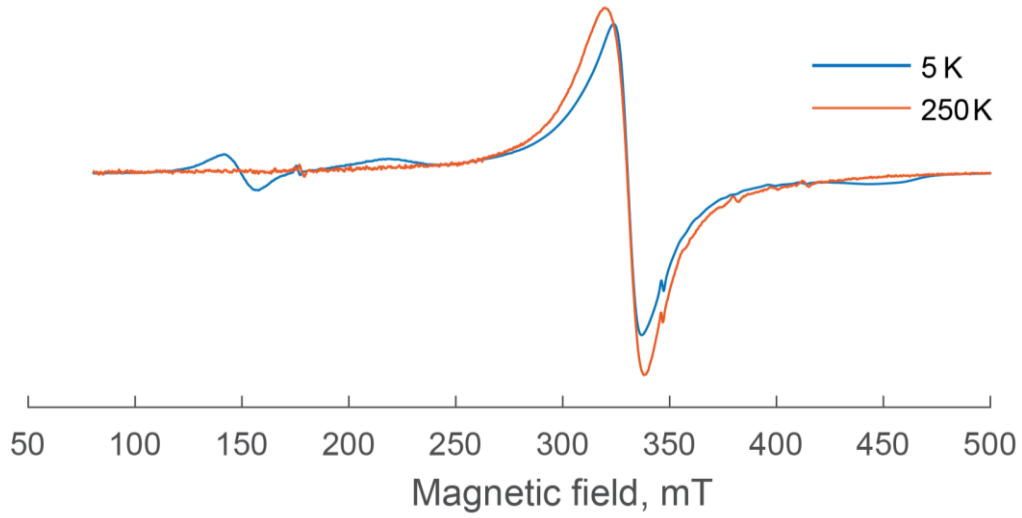

Fig. S3. EPR spectra of **I** measured above (250K) and below (5K) the temperature of magnetostructural SS↔WS transition (~ 141 K).

Figures S4 and S5 show the dynamics of EPR spectra of **I** and **II** during the experiment discussed in the main text. Legends show progression of the experiment in top-to-bottom order. Under cooling of the photoinduced WS state the spectrum of **I** retains its shape, but its intensity gradually rises upon reaching 5 K. In turn, **II** does have significant changes of EPR spectra in the cooling experiments.

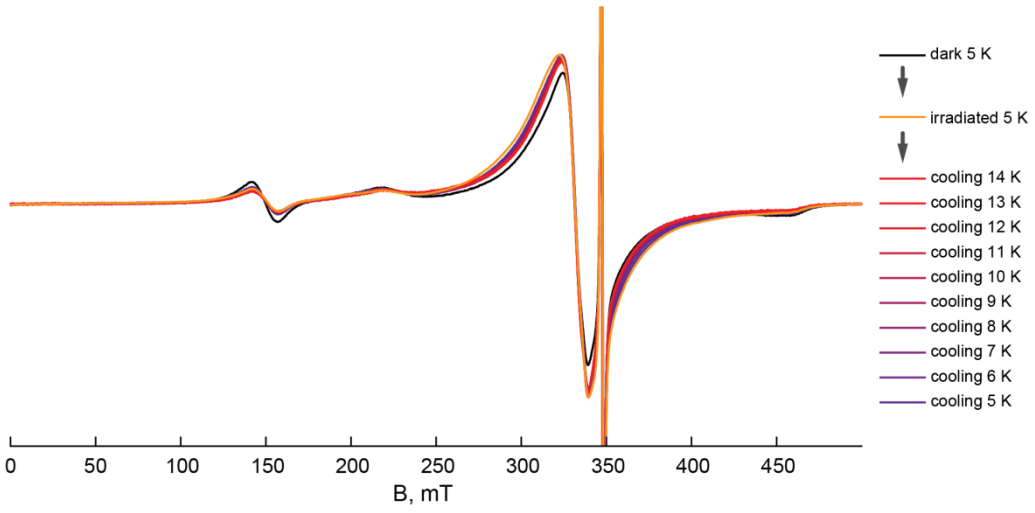

Fig. S4. EPR spectra of **I** measured under irradiation and consequent temperature changes. Legends show progression of the experiment in top-to-bottom order.

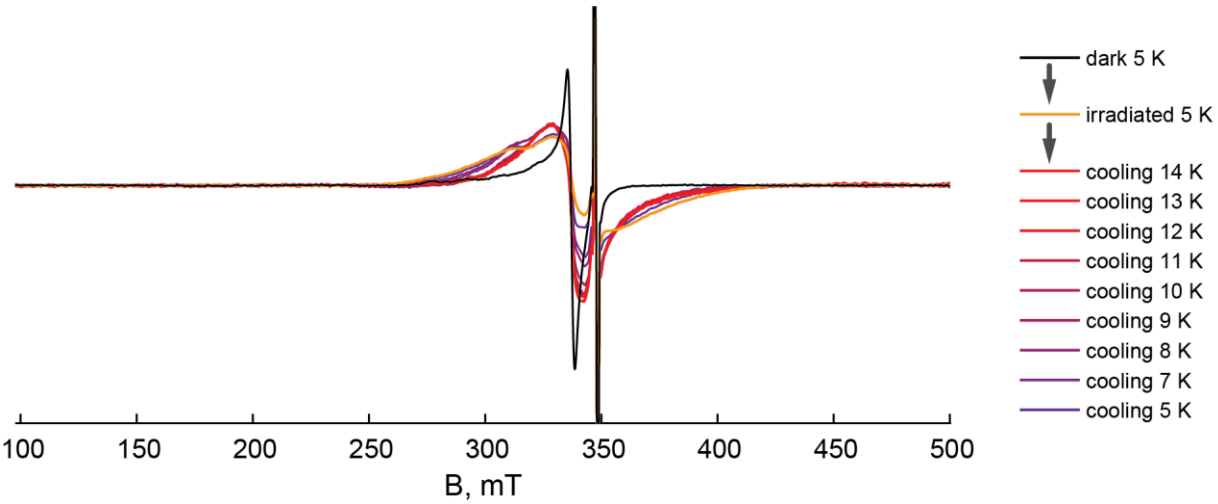

Fig. S5. EPR spectra of **II** measured under irradiation and consequent temperature changes. Legends show progression of the experiment in top-to-bottom order.

3. Evaluation of the accuracy of $I_2(T)$ measurements

In order to evaluate the final errors in the experiments on $I_2(T)$ measurement, we reproduced all results shown in Figure 5 for both compounds **I** and **II** using different (freshly prepared) samples. The superimposed results of two independent experiments are shown in Figures S6 and S7. One observes that the agreement between two experiments on compound **II** is very good (Fig. S7), and standard deviation between these two experiments is only ~0.01 (leading to negligible error bars in Figure 5b of the main text). For compound **I** (Fig. S6), signal-to-noise ratio is worse and therefore formal standard deviation is ~0.05 (visualized by error bars in Figure 5a). However, more important, the fitting of the $I_2(T)$ dependence with a constant function gives agreement with standard deviation of 0.007 only (Fig. S8). This means, that we can safely exclude the growth of $\chi T(T)$ by 0.05 – 0.10 (in the units of Figure 2a) anticipated for J~2-10 cm^{-1}.

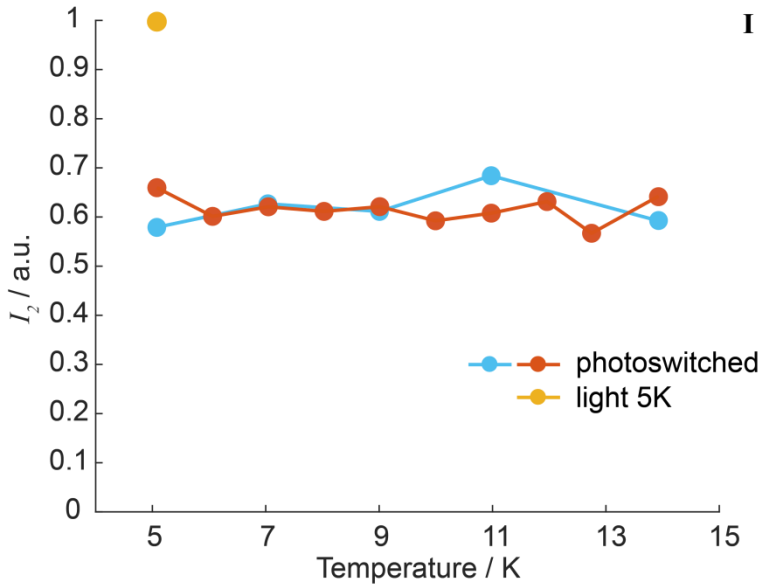

Fig. S6. $I_2(T)$ functions for compound **I** obtained in two independent measurements (shown in blue and red).

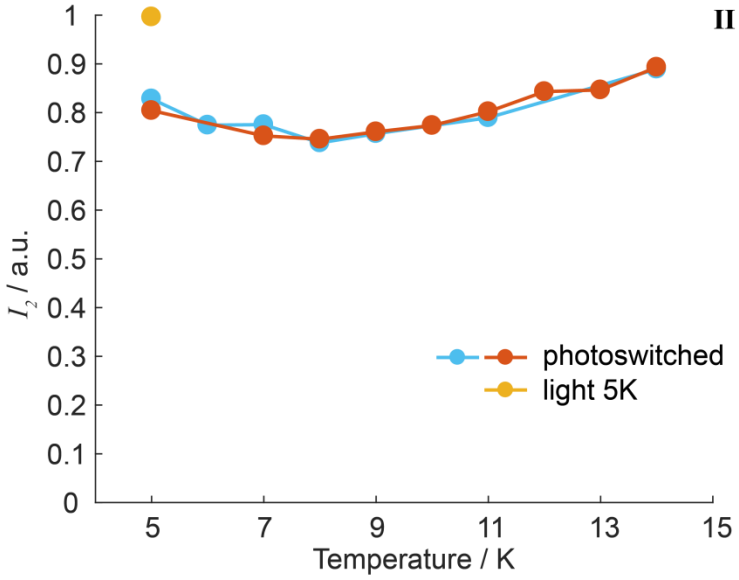

Fig. S7. $I_2(T)$ functions for compound **II** obtained in two independent measurements (shown in blue and red).

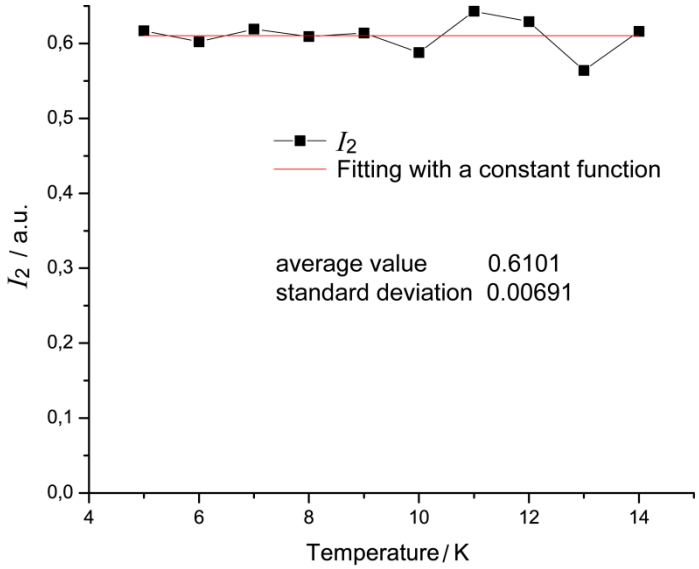

Fig. S8. Fitting of $I_2(T)$ for compound **I** (black) using a constant function (red). The constant (average) value and standard deviation are indicated. The experimental data is the average of two measurements shown in Fig. S6.